

Surface electron doping induced double gap opening in T_d-WTe_2

Qi-Yuan Li(李启远), Yang-Yang Lv(吕洋洋), Yong-Jie Xu(徐永杰), Li Zhu(朱立), Wei-Min Zhao(赵伟民), Yanbin Chen(陈延彬), and Shao-Chun Li(李绍春)

Citation: Chin. Phys. B, 2022, 31 (**6**): 066802. DOI: 10.1088/1674-1056/ac632e
Journal homepage: http://cpb.iphy.ac.cn; http://iopscience.iop.org/cpb

What follows is a list of articles you may be interested in

Realization of semiconducting Cu_2Se by direct selenization of Cu(111)

Yumu Yang(杨雨沐), Qilong Wu(吴奇龙), Jiaqi Deng(邓嘉琦), Jing Wang(王静), Yu Xia(夏雨), Xiaoshuai Fu(富晓帅), Qiwei Tian(田麒玮), Li Zhang(张力), Long-Jing Yin(殷隆晶), Yuan Tian(田园), Sheng-Yi Xie(谢声意), Lijie Zhang(张利杰), and Zhihui Qin(秦志辉)

Chin. Phys. B, 2021, 30 (**11**): 116802. DOI: 10.1088/1674-1056/ac0037

Phase transition-induced superstructures of *β*-Sn films with atomic-scale thickness

Le Lei(雷乐), Feiyue Cao(曹飞跃), Shuya Xing(邢淑雅), Haoyu Dong(董皓宇), Jianfeng Guo(郭剑锋), Shangzhi Gu(顾尚志), Yanyan Geng(耿燕燕), Shuo Mi(米烁), Hanxiang Wu(吴翰翔), Fei Pang(庞斐), Rui Xu(许瑞), Wei Ji(季威), and Zhihai Cheng(程志海)

Chin. Phys. B, 2021, 30 (**9**): 096804. DOI: 10.1088/1674-1056/ac11e8

NBN-doped nanographene embedded with five- and seven-membered rings on Au(111) surface

Huan Yang(杨欢), Yun Cao(曹云), Yixuan Gao(高艺璇), Yubin Fu(付钰彬), Li Huang(黄立), Junzhi Liu(刘俊治), Xinliang Feng(冯新亮), Shixuan Du(杜世萱), and Hong-Jun Gao(高鸿钧)

Chin. Phys. B, 2021, 30 (**5**): 056802. DOI: 10.1088/1674-1056/abeede

Epitaxial growth of antimony nanofilms on HOPG and thermal desorption to control the film thickness

Shuya Xing(邢淑雅), Le Lei(雷乐), Haoyu Dong(董皓宇), Jianfeng Guo(郭剑峰), Feiyue Cao(曹飞跃), Shangzhi Gu(顾尚志), Sabir Hussain, Fei Pang(庞斐), Wei Ji(季威), Rui Xu(许瑞), Zhihai Cheng(程志海)

Chin. Phys. B, 2020, 29 (**9**): 096801. DOI: 10.1088/1674-1056/aba27c

STM study of selenium adsorption on Au(111) surface

Bin Liu(刘斌), Yuan Zhuang(庄源), Yande Que(阙炎德), Chaoqiang Xu(徐超强), Xudong Xiao(肖旭东)

Chin. Phys. B, 2020, 29 (**5**): 056801. DOI: 10.1088/1674-1056/ab821d

---

Surface electron doping induced double gap opening in T_d-WTe_2

Qi-Yuan Li(李启远)[1,2], Yang-Yang Lv(吕洋洋)[1,3], Yong-Jie Xu(徐永杰)[1,2], Li Zhu(朱立)[1,2], Wei-Min Zhao(赵伟民)[1,2], Yanbin Chen(陈延彬)[1,2,4], and Shao-Chun Li(李绍春)[1,2,4,5,†]

[1] *National Laboratory of Solid State Microstructures, Nanjing University, Nanjing* 210093, *China*
[2] *School of Physics, Nanjing University, Nanjing* 210093, *China*
[3] *Department of Materials Science and Engineering, Nanjing University, Nanjing* 210093, *China*
[4] *Collaborative Innovation Center of Advanced Microstructures, Nanjing University, Nanjing* 210093, *China*
[5] *Jiangsu Provincial Key Laboratory for Nanotechnology, Nanjing University, Nanjing* 210093, *China*

(Received 18 January 2022; revised manuscript received 20 March 2022; accepted manuscript online 1 April 2022)

By using scanning tunneling microscopy, we investigated the electronic evolution of T_d-WTe_2 via *in-situ* surface alkali K atoms deposition. The T_d-WTe_2 surface is electron doped upon K deposition, and as the K coverage increases, two gaps are sequentially opened near Fermi energy, which probably indicates that two phase transitions concomitantly occur during electron doping. The two gaps both show a dome-like dependence on the K coverage. While the bigger gap shows no prominent dependence on the magnetic field, the smaller one can be well suppressed and thus possibly corresponds to the superconducting transition. This work indicates that T_d-WTe_2 exhibits rich quantum states closely related to the carrier concentration.

Keywords: scanning tunneling microscopy, T_d-WTe_2, surface electron doping, superconductivity transition

PACS: 68.37.Ef, 74.78.−w, 68.65.−k **DOI:** 10.1088/1674-1056/ac632e

1. Introduction

Layered transition metal dichalcogenides (TMDs) family exhibits various quantum states, such as spin density wave (SDW) state,[1] charge density wave (CDW) state,[2] superconducting (SC) phase,[3] two-dimensional (2D) quantum spin Hall (QSH) state,[4] and three-dimensional (3D) topological semimetal (TSM) state.[5–7] Tuning the superconducting transition in topological materials provides a promising way to search for the topological superconductors, and quite a few methods have been developed towards this target. For instance, superconductivity in topological materials can be realized by elements substitution,[8,9] high pressure,[10–13] atom intercalation,[14–19] gating,[20–24] proximity effect,[25–27] point contact,[28–32] etc.

As a particular example, T_d-WTe_2 hosts the type-II Weyl semimetal state in the bulk and undergoes superconductivity transition via atomic intercalation[5,15] or under high pressure.[10,11,33] It has initially attracted extensive research attention because of the giant unsaturated magnetoresistance that is possibly caused by the perfect compensation of electron and hole pockets at the Fermi level.[34–38] Later on, it was also predicted and confirmed as the type-II Weyl semimetal in the bulk[5,39–41] and quantum spin Hall state in the monolayer[4,42] respectively. Regarding to the mechanism of superconducting transition in WTe_2, several mechanisms have been proposed, such as the quantum phase transition[10] caused by the reconstruction of Fermi surface, the increased electronic density at Fermi level[11] caused by the lattice compression under high pressure, and the possible pressure-induced structural transition from T_d to $1T'$ phase.[33] For the case of electron doping induced superconductivity, it was theoretically indicated that the softening of phonons with the specific momentum, the relevant enhanced electron–phonon coupling, and the Fermi surface nesting may together drive the superconducting transition of WTe_2.[43] It was suggested that electronic doping can induce soft-mode phonon-mediated superconducting phase transitions and CDW phase transitions in WTe_2.[24,43] Angle-resolved photoelectron spectroscopy (ARPES) measurement also observed two quantum phase transitions in WTe_2 induced by surface electron doping.[44] To date, the detailed electronic evolution during electron doping in T_d-WTe_2 is still experimentally elusive.

In this study, we focused on the surface electronic doping in WTe_2 induced by *in situ* surface deposition of K atoms, and fully characterized the evolution of its electronic structures, via the measurement of local density of state (LDOS) near Fermi energy, by using scanning tunneling spectroscopy (STS). We found that electron doping induces two electronic phase transitions in WTe_2 and opens two energy gaps respectively. The first (larger) energy gap may be related a bosonic quantum phase transition, and the second (smaller) energy gap may correspond to the superconducting phase transition. Moreover, both of the energy gaps show a dome-shape dependence on the level of electron doping.

†Corresponding author. E-mail: scli@nju.edu.cn

© 2022 Chinese Physical Society and IOP Publishing Ltd

2. Experimental methods

Single crystal WTe_2 was grown by chemical vapor transport (CVT) method, the detailed growth conditions can refer to the literature.[39] After loading into the ultrahigh vacuum chamber (base pressure of 1×10^{-10} mbar), the pristine WTe_2 surface was obtained by *in-situ* cleaving the WTe_2 single crystal at room temperature. The cleaved surface quality was checked by STM. The K atoms were deposited on the clean WTe_2 surface kept at low temperature. After K deposition, the sample was immediately transferred back to the STM stage for scan without annealing. Scanning tunneling microscopy/spectroscopy (STM/STS) measurements were performed at liquid helium temperature (~ 4.2 K) with a commercial scanning tunneling microscope (Unisoku, USM1300). STM topographic images were acquired under the constant current mode, and STS $\mathrm{d}I/\mathrm{d}V$ spectra were taken with a lock-in amplifier and a typical ac modulation of $\sim$ 1–10 mV at 963 Hz.

3. Results and discussion

T_d-WTe_2 is a typical layered van der Waals material, and its bulk form is in the T_d phase with an octahedral structure, a distorted $1T$ phase, as illustrated in Fig. 1(a). The STM topographic image taken on the cleaved pristine WTe_2 surface, as shown in Fig. 1(b), gives clearly the positions of the topmost Te atoms. The STS spectrum, as shown in Fig. 1(c), indicates that there exists the residual intensity at the Fermi energy, confirming its semi-metallic nature, which is consistent with the previous STM studies.[45–47] The characteristic bump at the positive bias of +0.62 V, as marked in Fig. 1(c), can be used as the reference to determine the level of electron doping.

The surface morphologies of WTe_2 after depositing different coverages of K atoms are shown in Figs. 2(a)–2(c), and supplementary information. When the K coverage is low,

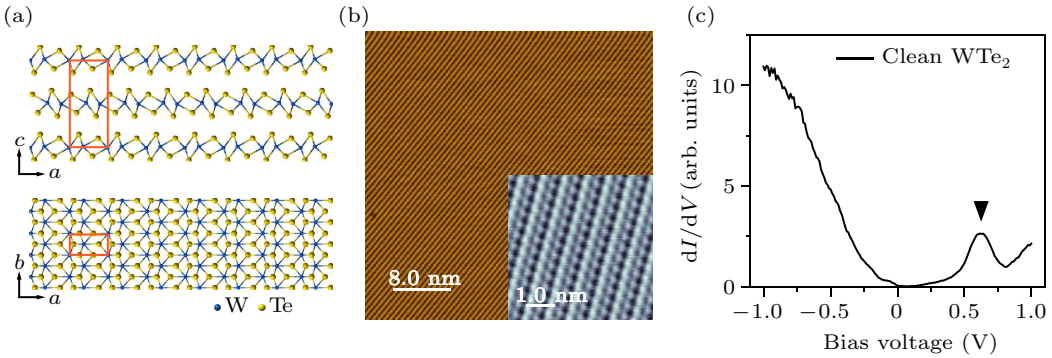


Fig. 1. STM and STS results taken on the pristine T_d-WTe_2 surface. (a) Atomic structure of bulk T_d-WTe_2. (b) STM topographic image (40×40 nm^2) of the pristine T_d-WTe_2 surface. $U = +1.0$ V, $I_t = 100$ pA. Inset: the atomic resolution image (5×5 nm^2). $U = +5.0$ mV, $I_t = 140$ pA. (c) $\mathrm{d}I/\mathrm{d}V$ spectrum taken on the pristine surface of T_d-WTe_2 (set point: $U = +1.0$ V, $I_t = 200$ pA).

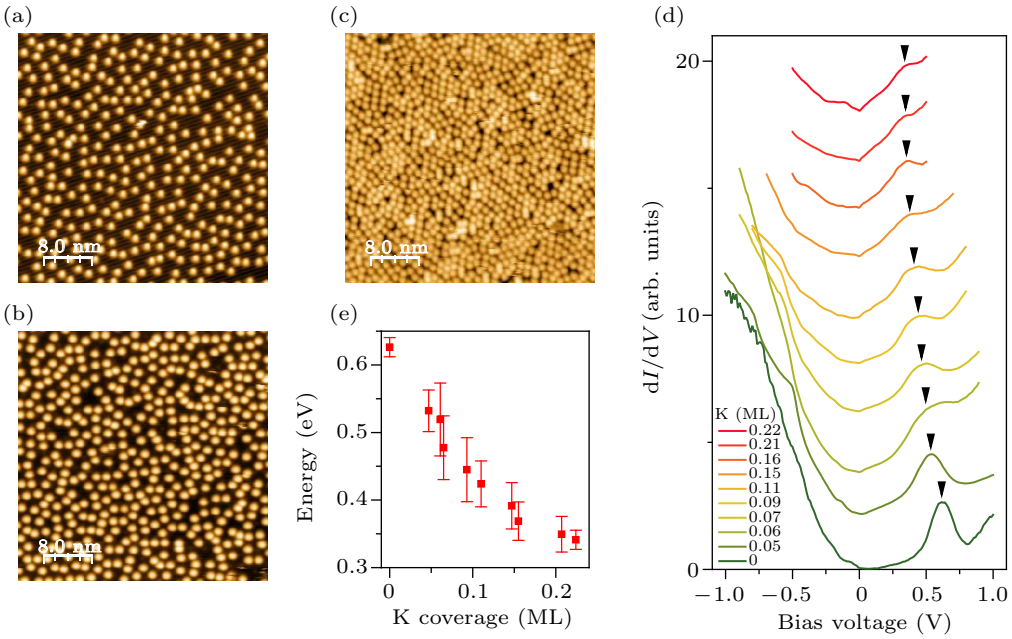


Fig. 2. STM and STS results taken on the T_d-WTe_2 surface with deposited surface K atoms. (a)–(c) STM topographic images (40×40 nm^2) at the surface with the K coverages of ~ 0.05 ML, ~ 0.06 ML and ~ 0.09 ML, respectively. $U = +1.0$ V, $I_t = 100$ pA. (d) $\mathrm{d}I/\mathrm{d}V$ spectra taken on the T_d-WTe_2 surface with various K coverages ranging from 0 to ~ 0.22 ML. (setpoint: $U = +1.0$ V, $I_t = 200$ pA). The triangle in (d) is used to mark the position of the characteristic bump as a reference to determine the Fermi level shift. (e) Statistical result showing the dependence of the characteristic bump position on the K coverage.

as shown in Fig. 2(a), the K atoms prefer to adsorb on the position between Te atomic chains, and are randomly distributed on the surface. As the K coverage increases, the K atoms in sequence form series of ordered structures, from the hexagonal arrangement at ~ 0.16 ML to the tetragonal at ~ 0.29 ML, as shown in supplementary information. These ordered structures of K atoms show weak dependence on the lattice symmetry of the WTe_2 substrate. The STS spectra taken on these surfaces with difference K coverages are shown in Fig. 2(d). As the K coverage increases, the position of the characteristic bump, as marked by the triangular arrow in Fig. 2(d), moves systematically towards the left, indicating that the Fermi level is shifted upward, and the electron doping indeed occurs at the WTe_2 surface. Figure 2(e) summarizes the statistical results of the Fermi energy shift versus the K atom coverage, as indicated by the position of the characteristic bump. A total shift of ~ 285 mV was achieved within our experimental set up. In the case of low K coverage, the electron doping is very efficient since the characteristic bump moves greatly, while as the K coverage increases, the electron doping gradually approaches a saturation. When the coverage of K atom reaches to ~ 0.21 ML, the characteristic peak of STS spectrum does not obviously change.

We measured the STS spectra in a small bias voltage to investigate the electronic evolution at the Fermi energy. Figure 3(a) shows the STS spectra taken within ± 100 mV. A V-shaped energy gap starts to appear near the Fermi energy at the K coverage of ~ 0.05 ML, and is always kept as the K coverage increases. This energy gap, namely, the first gap, is located right along the Fermi energy. To further quantitatively investigate the detailed evolution of the energy gap, we took the STS spectra at a smaller bias voltage range within ± 20 mV, as shown in Fig. 3(b). Surprisingly, as the K coverage increases to ~ 0.09 ML, a second energy gap of ~ 3.4 mV starts to appear near the Fermi energy as well, which is smaller than the first one. The peak positions of the two energy gaps are marked by blue and red triangles in Figs. 3(b) and 3(c), respectively. Two representative STS spectra are highlighted in Fig. 3(c), to make a comparison between the case with only the first and with both of the gaps. We point out that there exists a slight variation in the STS spectra, which is possibly due to the surface inhomogeneity of local electron doping, see supplementary Fig. S3. By checking many STS data taken on various locations of the WTe_2 surface, we identify that the second feature is an energy gap instead of a kink or a hump. But the second energy gap is not very obvious that is possibly due to the thermal broadening at 4.2 K, a comparable temperature to the expected T_c for superconducting WTe_2.[15] Figure 3(d) summarizes the dependence of the two energy gaps on the electron doping level (as indicated by the K coverage). As the K coverage increases, the two energy gaps gradually increase in size to reach a maximum at ~ 0.22 ML (the first gap) and at ~ 0.16 ML (the second gap), respectively. As the K coverage further increases, the two energy gaps decrease in size, but are both persistent in the whole explored coverage range. The two energy gaps show a dome-shape like dependence on the K coverage, which is similar to the phase diagram of WTe_2 superconductivity caused by high pressure and atom intercalation.[10,11,15]

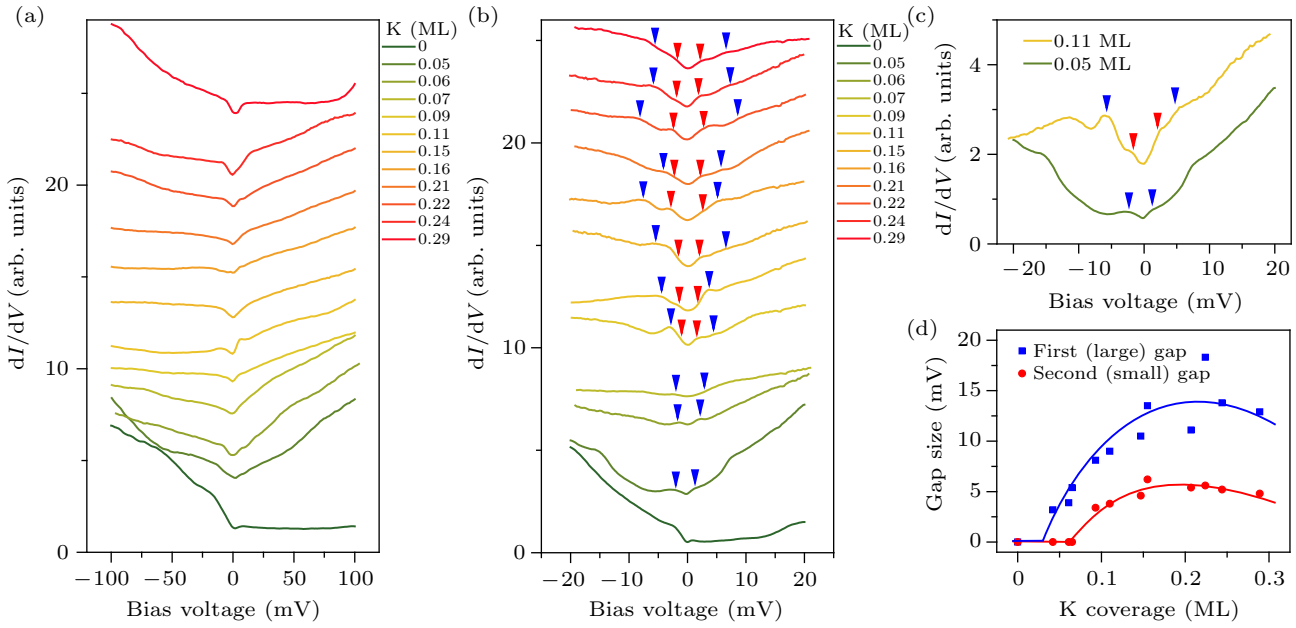


Fig. 3. Spectral evolution near the Fermi energy via surface K deposition. (a) STS dI/dV spectra taken within the bias range from -100 mV to $+100$ mV. Setpoint: $U = +100$ mV, $I_t = 200$ pA. (b) STS dI/dV spectra taken within the bias range from -20 mV to $+20$ mV. Setpoint: $U = +20$ mV, $I_t = 200$ pA. The blue and red triangular arrows in (b) mark the peak positions of the first energy gap and the second energy gap, respectively. (c) Two representative STS dI/dV spectra taken at K coverage of 0.05 ML and 0.11 ML, showing clearly the first energy gap and the second energy gap, as marked by blue and red triangle arrows, respectively (d) Statistical result showing that the two energy gap sizes vary with K coverage.

In order to unveil the physical nature of the two energy gaps, we chose the T_d-WTe_2 surface covered by ~ 0.09 ML of K atoms to explore the spectroscopic evolution under magnetic field. Figure 4(a) shows the STS spectra taken under the various vertical magnetic field up to 9 T. To quantitatively demonstrate the evolution of the second gap upon magnetic field, we measured the intensities at the coherence peak and zero bias, as shown in Fig. 4(b). In particular, the value of the peak minus zero bias intensity, as shown by the red dots in Fig. 4(b), shows a clear trend of decrease upon increasing the magnetic field. There exists background variation outside the two energy gaps, the origin of which is very complicated and not the focus of this work. The background was subtracted in order to clearly identify the two energy gaps, as shown in supplementary Fig. S2. The first energy gap shows no prominent magnetic field-induced spectral change. In contrast, the intensity of the coherence peaks for the second energy gap is gradually suppressed upon the increase of the magnetic field. We note that the right-hand side peak for the second gap is difficult to identify due to the convolution with the first gap. Meanwhile the STS intensity at zero bias is increased as well. Even though a BCS fit to the energy gap would expectedly give a reduced gap size under the magnetic field, we did not make such a quantitative analysis because the gap is relatively small comparing to the thermal broadening, and the error bar for the fitting should be too large to be scientifically reasonable.

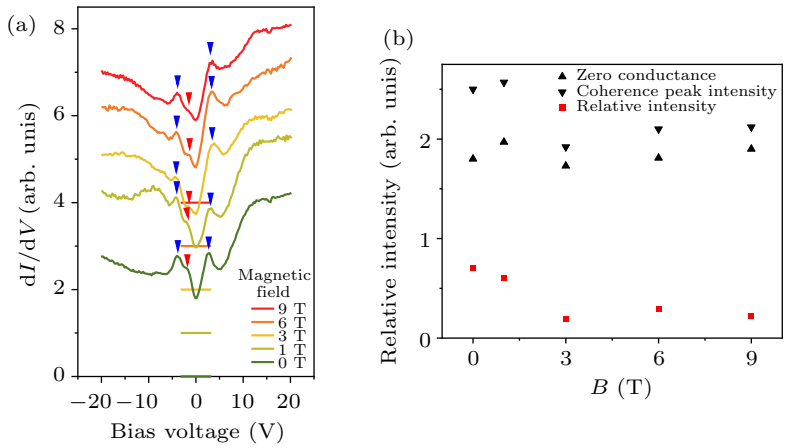


Fig. 4. Dependence of the STS dI/dV spectra on the applied magnetic field. (a) STS dI/dV spectra acquired at different magnetic fields. (b) The dependence of coherence peak and spectral intensity at zero bias and their relative intensity on the magnetic field. The magnetic field is perpendicular to the sample surface and the maximum magnetic field applied is 9 T. The dI/dV spectra were taken at the setpoint of $U = +20$ mV and $I_t = 200$ pA. The first and second energy gaps are marked by blue and red triangle arrows, respectively.

In the following, we discuss some other possible origins for this small energy gap. In addition to the superconducting transition, previous theoretical calculations indicated that a CDW phase transition may be also induced by electron doping, which requires more electron doping than the superconducting transition.[43] But the case that a CDW gap usually does not change under the magnetic field is inconsistent with our results. Previous ARPES measurement also indicated two quantum phase transitions in WTe_2 upon surface electron doping,[44] but neither of the two transitions would induce an energy gap pinned at Fermi energy, inconsistent with our observation as well. A pseudogap may also appear concomitantly, as a precursor of superconducting transition,[48] but the pseudogap does not change with the magnetic field as well. Therefore, we believe that it is most likely that the second energy gap corresponds to the superconducting transition. We have to point out that to undoubtedly demonstrate the physical nature of the first energy gap requires further extensive explorations.

Previous ARPES study[44] has observed two nonmonotonic phase transitions in WTe_2 during the surface electron doping. The first transition was tentatively interpreted by a metastable shear displacement of the topmost WTe_2 layer, and the second one by the coupling between alkali dopants and the host through hybridization and the surface dipole electric field generated by the positive K ions and negative WTe_2 electrons. In our study, when the first gap opens, we did not observe a shear displacement of the top WTe_2 layer, which would otherwise cause the formation of a moire pattern. The electric field of dipole formed by the ironized K atom and WTe_2 would reduce the single particle band gap, in contrast with our observation. Considering our observation that the energy gap has two coherence peaks and symmetrically locate at the Fermi energy, it must be a many-body gap. Even though the origin is not clear, it is not likely an excitonic insulating gap which would be enlarged at the presence of surface K dipole layer, because the gap is robust against the surface electron doping, in contrast with the behavior of the excitonic insulator gap.[49] It is also not excluded that the first gap corresponds to the bosonic mode excitation, for instance the phonon mode as proposed in modulating the superconductivity transition in monolayer WTe_2. Further extended work is required to unveil the nature of the first gap.

4. Conclusion

In summary, we realized the surface electron doping in WTe_2 via deposition of alkali atoms, and accordingly tuned the Fermi energy. Two energy gaps are formed sequentially near Fermi energy as the electron doping increases. Even though the origin of the first (large) gap is still not known, it may correspond to a many-body state. The second (small) gap can be suppressed by applied magnetic field, thus indicating a superconducting gap. Both of the energy gaps show a dome-like dependence on the level of electron doping, possibly suggestive of the unconventional superconductivity mechanism.

Acknowledgements

We thank Dr. Ping Zhang and Dr. Fawei Zheng for fruitful discussions. This work was financially supported by the National Natural Science Foundation of China (Grants Nos. 11790311, 92165205, 51902152, 11874210, and 11774149) and the National Key R&D Program of China (Grants No. 2021YFA1400403).

References

[1] Law K T and Lee P A 2017 *Proc. Natl. Acad. Sci. USA* **114** 6996
[2] Wang L, Wu Y, Yu Y, Chen A, Li H, Ren W, Lu S, Ding S, Yang H, Xue Q K, Li F S and Wang G 2020 *ACS Nano* **14** 8299
[3] Wilson J A and Yoffe A D 1969 *Adv. Phys.* **18** 193
[4] Qian X, Liu J, Fu L and Li J 2014 *Science* **346** 1344
[5] Soluyanov A A, Gresch D, Wang Z, Wu Q, Troyer M, Dai X and Bernevig B A 2015 *Nature* **527** 495
[6] Haldane F D 2004 *Phys. Rev. Lett.* **93** 206602
[7] Shuichi M 2007 *New J. Phys.* **9** 356
[8] Liu Y, Shao D F, Li L J, Lu W J, Zhu X D, Tong P, Xiao R C, Ling L S, Xi C Y, Pi L, Tian H F, Yang H X, Li J Q, Song W H, Zhu X B and Sun Y P 2016 *Phys. Rev. B* **94** 045131
[9] Chen F C, Luo X, Xiao R C, Lu W J, Zhang B, Yang H X, Li J Q, Pei Q L, Shao D F, Zhang R R, Ling L S, Xi C Y, Song W H and Sun Y P 2016 *Appl. Phys. Lett.* **108** 162601
[10] Kang D, Zhou Y, Yi W, Yang C, Guo J, Shi Y, Zhang S, Wang Z, Zhang C, Jiang S, Li A, Yang K, Wu Q, Zhang G, Sun L and Zhao Z 2015 *Nat. Commun.* **6** 7804
[11] Pan X C, Chen X, Liu H, Feng Y, Wei Z, Zhou Y, Chi Z, Pi L, Yen F, Song F, Wan X, Yang Z, Wang B, Wang G and Zhang Y 2015 *Nat. Commun.* **6** 7805
[12] Qi Y, Naumov P G, Ali M N, Rajamathi C R, Schnelle W, Barkalov O, Hanfland M, Wu S C, Shekhar C, Sun Y, Suss V, Schmidt M, Schwarz U, Pippel E, Werner P, Hillebrand R, Forster T, Kampert E, Parkin S, Cava R J, Felser C, Yan B and Medvedev S A 2016 *Nat. Commun.* **7** 11038
[13] Sipos B, Kusmartseva A F, Akrap A, Berger H, Forro L and Tutis E 2008 *Nat. Mater.* **7** 960
[14] Zhang R, Tsai I L, Chapman J, Khestanova E, Waters J and Grigorieva I V 2016 *Nano Lett.* **16** 629
[15] Zhu L, Li Q Y, Lv Y Y, Li S, Zhu X Y, Jia Z Y, Chen Y B, Wen J S and Li S C 2018 *Nano Lett.* **18** 6585
[16] Hor Y S, Williams A J, Checkelsky J G, Roushan P, Seo J, Xu Q, Zandbergen H W, Yazdani A, Ong N P and Cava R J 2010 *Phys. Rev. Lett.* **104** 057001
[17] Kriener M, Segawa K, Ren Z, Sasaki S, Wada S, Kuwabata S and Ando Y 2011 *Phys. Rev. B* **84** 054513
[18] Liao M, Wang H, Zhu Y, Shang R, Rafique M, Yang L, Zhang H, Zhang D and Xue Q K 2021 *Nat. Commun.* **12** 5342
[19] Wang Z, Li R, Su C and Loh K P 2020 *SmartMat* **1** e1013
[20] Yu Y, Yang F, Lu X F, Yan Y J, Cho Y H, Ma L, Niu X, Kim S, Son Y W, Feng D, Li S, Cheong S W, Chen X H and Zhang Y 2015 *Nat. Nanotechnol.* **10** 270
[21] Fatemi V, Wu S, Cao Y, Bretheau L, Gibson Q D, Watanabe K, Taniguchi T, Cava R J and Jarillo-Herrero P 2018 *Science* **362** 926
[22] Sajadi E, Palomaki T, Fei Z, Zhao W, Bement P, Olsen C, Luescher S, Xu X, Folk J A and Cobden D H 2018 *Science* **362** 922
[23] Piatti E, De Fazio D, Daghero D, Tamalampudi S R, Yoon D, Ferrari A C and Gonnelli R S 2018 *Nano Lett.* **18** 4821
[24] Lee J H and Son Y W 2021 *Phys. Chem. Chem. Phys.* **23** 17279
[25] Li Q, He C, Wang Y, Liu E, Wang M, Wang Y, Zeng J, Ma Z, Cao T, Yi C, Wang N, Watanabe K, Taniguchi T, Shao L, Shi Y, Chen X, Liang S J, Wang Q H and Miao F 2018 *Nano Lett.* **18** 7962
[26] Lüpke F, Waters D, De La Barrera S C, Widom M, Mandrus D G, Yan J, Feenstra R M and Hunt B M 2020 *Nat. Phys.* **16** 526
[27] Huang C, Narayan A, Zhang E, Liu Y, Yan X, Wang J, Zhang C, Wang W, Zhou T, Yi C, Liu S, Ling J, Zhang H, Liu R, Sankar R, Chou F, Wang Y, Shi Y, Law K T, Sanvito S, Zhou P, Han Z and Xiu F 2018 *ACS Nano* **12** 7185
[28] Wang H, Wang H, Liu H, Lu H, Yang W, Jia S, Liu X J, Xie X C, Wei J and Wang J 2016 *Nat. Mater.* **15** 38
[29] Aggarwal L, Gaurav A, Thakur G S, Haque Z, Ganguli A K and Sheet G 2016 *Nat. Mater.* **15** 32
[30] Wang H, Ma L and Wang J 2018 *Sci. Bull.* **63** 1141
[31] Hou X Y, Wang Z, Gu Y D, He J B, Chen D, Zhu W L, Zhang M D, Zhang F, Xu Y F, Zhang S, Yang H X, Ren Z A, Weng H M, Hao N, Lv W G, Hu J P, Chen G F and Shan L 2019 *Phys. Rev. B* **100** 235109
[32] Hou X Y, Gu Y D, Li S J, Zhao L X, Zhu W L, Wang Z, Zhang M D, Zhang F, Zhang L, Zi H, Wu Y W, Yang H X, Ren Z A, Zhang P, Chen G F, Hao N and Shan L 2020 *Phys. Rev. B* **101** 134503
[33] Lu P C, Kim J S, Yang J, Gao H, Wu J F, Shao D X, Li B, Zhou D W, Sun J, Akinwande D J, Xing D Y and Lin J F 2016 *Phys. Rev. B* **94** 224512
[34] Ali M N, Xiong J, Flynn S, Tao J, Gibson Q D, Schoop L M, Liang T, Haldolaarachchige N, Hirschberger M, Ong N P and Cava R J 2014 *Nature* **514** 205
[35] Lv H Y, Lu W J, Shao D F, Liu Y, Tan S G and Sun Y P 2015 *Europhys. Lett.* **110** 37004
[36] Jiang J, Tang F, Pan X C, Liu H M, Niu X H, Wang Y X, Xu D F, Yang H F, Xie B P, Song F Q, Dudin P, Kim T K, Hoesch M, Das P K, Vobornik I, Wan X G and Feng D L 2015 *Phys. Rev. Lett.* **115** 166601
[37] Chen Y Q, Chen Y D, Ning J A, Chen L M, Zhuang W Z, He L, Zhang R, Xu Y B and Wang X F 2020 *Chin. Phys. Lett.* **37** 017104
[38] Chen Y Q, Liu R X, Chen Y D, Yuan X, Ning J, Zhang C C, Chen L M, Wang P, He L, Zhang R, Xu Y B and Wang X F 2021 *Chin. Phys. Lett.* **38** 017101
[39] Lv Y Y, Li X, Zhang B B, Deng W Y, Yao S H, Chen Y B, Zhou J, Zhang S T, Lu M H, Zhang L, Tian M, Sheng L and Chen Y F 2017 *Phys. Rev. Lett.* **118** 096603
[40] Wang Y, Liu E, Liu H, Pan Y, Zhang L, Zeng J, Fu Y, Wang M, Xu K, Huang Z, Wang Z, Lu H Z, Xing D, Wang B, Wan X and Miao F 2016 *Nat. Commun.* **7** 13142
[41] Deng K, Wan G, Deng P, Zhang K, Ding S, Wang E, Yan M, Huang H, Zhang H, Xu Z, Denlinger J, Fedorov A, Yang H, Duan W, Yao H, Wu Y, Fan S, Zhang H, Chen X and Zhou S 2016 *Nat. Phys.* **12** 1105
[42] Jia Z Y, Song Y H, Li X B, Ran K J, Lu P C, Zheng H J, Zhu X Y, Shi Z Q, Sun J, Wen J S, Xing D Y and Li S C 2017 *Phys. Rev. B* **96** 041108
[43] Yang W, Mo C J, Fu S B, Yang Y, Zheng F W, Wang X H, Liu Y A, Hao N and Zhang P 2020 *Phys. Rev. Lett.* **125** 237006
[44] Rossi A, Resta G, Lee S H, Redwing R D, Jozwiak C, Bostwick A, Rotenberg E, Savrasov S Y and Vishik I M 2020 *Phys. Rev. B* **102** 121110
[45] Zhang W, Wu Q, Zhang L, Cheong S W, Soluyanov A A and Wu W 2017 *Phys. Rev. B* **96** 165125
[46] Yuan Y, Yang X, Peng L, Wang Z J, Li J, Yi C J, Xian J J, Shi Y G and Fu Y S 2018 *Phys. Rev. B* **97** 165435
[47] Li Q, Yan J, Yang B, Zang Y, Zhang J, He K, Wu M, Zhao Y, Mandrus D, Wang J, Xue Q, Chi L, Singh D J and Pan M 2016 *Phys. Rev. B* **94** 115419
[48] Zhang K W, Yang C L, Lei B, Lu P C, Li X B, Jia Z Y, Song Y H, Sun J, Chen X H, Li J X and Li S C 2018 *Sci. Bull.* **63** 426
[49] Jia Y Y, Wang P J, Chiu C L, Song Z D, Yu G, Jäck B, Lei S M, Klemenz S, Cevallos F A, Onyszczak M, Fishchenko N, Liu X M, Farahi G, Xie F, Xu Y F, Watanabe K, Taniguchi T, Bernevig B A, Cava R J, Schoop L M, Yazdani A and Wu S F 2021 *Nat. Phys.* **18** 87